

Constraints on general primordial non-Gaussianity using wavelets for the Wilkinson Microwave anisotropy probe 7-year data

A. Curto,¹ * E. Martínez-González,¹ R. B. Barreiro,¹ M. P. Hobson²

¹ *Instituto de Física de Cantabria, CSIC-Universidad de Cantabria, Avda. de los Castros s/n, 39005 Santander, Spain.*

² *Astrophysics Group, Cavendish Laboratory, Madingley Road, Cambridge, CB3 0HE, U.K.*

Accepted Received ; in original form

ABSTRACT

We present constraints on the non-linear coupling parameter f_{nl} with the Wilkinson Microwave Anisotropy Probe (WMAP) data. We use the method based on the spherical Mexican hat wavelet (SMHW) to measure the f_{nl} parameter for three of the most interesting shapes of primordial non-Gaussianity: *local*, *equilateral* and *orthogonal*. Our results indicate that this parameter is compatible with a Gaussian distribution within the two sigma confidence level (CL) for the three shapes and the results are consistent with the values presented by the WMAP team. We have included in our analysis the impact on f_{nl} due to contamination by unresolved point sources. The point sources add a positive contribution of $\Delta f_{nl}^{loc} = 2.5 \pm 3.0$, $\Delta f_{nl}^{eq} = 37 \pm 18$ and $\Delta f_{nl}^{ort} = 25 \pm 14$. As mentioned by the WMAP team, the contribution of the point sources to the orthogonal and equilateral form is expected to be larger than to the local one and thus it cannot be neglected in future constraints on these parameters. Taking into account this contamination, our best estimates for f_{nl} are $-16.0 \leq f_{nl}^{loc} \leq 76.0$, $-382 \leq f_{nl}^{eq} \leq 202$ and $-394 \leq f_{nl}^{ort} \leq 34$ at 95% CL. The three shapes are compatible with zero at 95% CL (2σ). Our conclusion is that the WMAP 7-year data are consistent with Gaussian primordial fluctuations within 2σ CL. We stress however the importance of taking into account the unresolved point sources in the measurement of f_{nl} in future works, especially when using more precise data sets such as the forthcoming Planck data.

Key words: methods: data analysis - cosmic microwave background

1 INTRODUCTION

During the period of inflationary expansion in the very early stages of the universe, primordial perturbations were generated that are the seeds of the structures that we can observe today (Starobinskii 1979; Guth 1981; Albrecht & Steinhardt 1982; Linde 1982, 1983; Mukhanov et al. 1992). These primordial perturbations were linearly imprinted in the Cosmic Microwave Background (CMB) anisotropies. Thus the study of the CMB anisotropies is a powerful way to understand the physics of the early universe. Many observational CMB projects, for example the NASA WMAP¹ and ESA Planck² missions, different ground based 3D observational

campaigns of large scale structure and high energy accelerators are enabling us to understand better the properties and the evolution of the universe. From the several observational approaches that are available, the search for departures from Gaussianity in the CMB anisotropies with a primordial origin has become a powerful way to discriminate among different inflationary scenarios. Inflationary models such as the widely accepted standard, single-field, slow roll inflation predict low levels of non-Gaussianity whereas other models predict levels of non-Gaussianity that may be detected using the data from current experiments (Bartolo et al. 2004; Komatsu 2009; Yadav & Wandelt 2010; Komatsu 2010). A detection of a deviation from Gaussianity with a primordial origin would rule out many inflationary models and would have far reaching implications in the physics of the early universe.

* e-mail: curto@ifca.unican.es

¹ <http://map.gsfc.nasa.gov/>

² <http://www.esa.int/planck>

The level of primordial non-Gaussianity is usually

parametrised by the non-linear coupling parameter f_{nl} (Verde et al. 2000; Komatsu & Spergel 2001; Bartolo et al. 2004). This parameter measures departures from zero in the values of the third order quantity known as the bispectrum, characterised through the shape function $F(k_1, k_2, k_3)$. The bispectrum is related to Bardeen's curvature perturbations $\Phi(\mathbf{k})$ through the 3-point correlation function $\langle \Phi(\mathbf{k}_1)\Phi(\mathbf{k}_2)\Phi(\mathbf{k}_3) \rangle = (2\pi)^3 \delta^3(\mathbf{k}_1 + \mathbf{k}_2 + \mathbf{k}_3) F(k_1, k_2, k_3)$. Depending on the physical mechanisms of the different inflationary models the shape function can take different forms.

In this paper we measure the levels of non-Gaussianity present in the WMAP data corresponding to the three particular shapes (local, equilateral and orthogonal) that have been studied by the WMAP team (Komatsu et al. 2011). The shape function $F(k_1, k_2, k_3)$ of these types of non-Gaussianity, their CMB angular bispectra $b_{\ell_1 \ell_2 \ell_3}$ and the inflationary scenarios that generate these non-Gaussianity are described below.

- **Local shape.** Significant non-Gaussianity of the local form can be generated for example in multi-field inflationary models (Komatsu et al. 2005; Komatsu 2010), the curvaton model (Lyth et al. 2003), the inhomogeneous reheating scenario (Dvali et al. 2004; Bartolo et al. 2004), models based on hybrid inflation (Lin 2009), etc. This shape is given by (see for example Creminelli et al. 2006; Fergusson et al. 2010a; Yadav & Wandelt 2010; Komatsu et al. 2011)

$$F(k_1, k_2, k_3) = 2A^2 f_{nl} \left[\frac{1}{k_1^{3-(n_s-1)} k_2^{3-(n_s-1)}} + \frac{1}{k_1^{3-(n_s-1)} k_3^{3-(n_s-1)}} + \frac{1}{k_2^{3-(n_s-1)} k_3^{3-(n_s-1)}} \right], \quad (1)$$

and its angular bispectrum is (see for example Fergusson et al. 2010a; Yadav & Wandelt 2010; Komatsu 2010)

$$b_{\ell_1 \ell_2 \ell_3}^{loc} = 2 \int_0^\infty x^2 dx \left[\alpha_{\ell_1}(x) \beta_{\ell_2}(x) \beta_{\ell_3}(x) + \beta_{\ell_1}(x) \alpha_{\ell_2}(x) \beta_{\ell_3}(x) + \beta_{\ell_1}(x) \beta_{\ell_2}(x) \alpha_{\ell_3}(x) \right], \quad (2)$$

where A is the amplitude of the power spectrum $P_\Phi(k) = Ak^{n_s-4}$, n_s is the spectral index and $\alpha_\ell(x)$, $\beta_\ell(x)$ are filter functions (see for example Komatsu & Spergel 2001; Komatsu et al. 2005; Fergusson et al. 2010a; Komatsu 2010).

- **Equilateral shape.** Significant non-Gaussianity of the equilateral form can be generated for example by the Dirac-Born-Infeld inflation (Silverstein & Tong 2004; Bartolo et al. 2004; Langlois et al. 2008), ghost inflation (Arkani-Hamed et al. 2004), several single-field inflationary models in Einstein gravity (Chen et al. 2007) etc. This shape is given by (see for example Creminelli et al. 2006; Fergusson et al. 2010a; Yadav & Wandelt 2010; Komatsu et al. 2011)

$$F(k_1, k_2, k_3) = 6A^2 f_{nl} \left[-\frac{1}{k_1^{3-(n_s-1)} k_2^{3-(n_s-1)}} - \frac{1}{k_1^{3-(n_s-1)} k_3^{3-(n_s-1)}} - \frac{1}{k_2^{3-(n_s-1)} k_3^{3-(n_s-1)}} - \frac{2}{(k_1 k_2 k_3)^{2(4-n_s)/3}} \right]$$

$$+ \left\{ \frac{1}{k_1^{(4-n_s)/3} k_2^{2(4-n_s)/3} k_3^{(4-n_s)}} + (5 \text{ perm}) \right\}, \quad (3)$$

and its angular bispectrum is (see for example Fergusson et al. 2010a; Yadav & Wandelt 2010; Komatsu 2010)

$$b_{\ell_1 \ell_2 \ell_3}^{eq} = 6 \int_0^\infty dx x^2 \left[-\alpha_{\ell_1}(x) \beta_{\ell_2}(x) \beta_{\ell_3}(x) + (2 \text{ perm}) + \beta_{\ell_1}(x) \gamma_{\ell_2}(x) \delta_{\ell_3}(x) + (5 \text{ perm}) - 2\delta_{\ell_1}(x) \delta_{\ell_2}(x) \delta_{\ell_3}(x) \right], \quad (4)$$

where $\gamma_\ell(x)$ and $\delta_\ell(x)$ are filter functions (see for example Fergusson et al. 2010a; Komatsu 2010).

- **Orthogonal shape.** Significant non-Gaussianity of the orthogonal form can be generated in general single-field models (Cheung et al. 2008; Senatore et al. 2010). This shape is given by (see for example Senatore et al. 2010; Yadav & Wandelt 2010; Komatsu et al. 2011)

$$F(k_1, k_2, k_3) = 6A^2 f_{nl} \left[-\frac{3}{k_1^{3-(n_s-1)} k_2^{3-(n_s-1)}} - \frac{3}{k_1^{3-(n_s-1)} k_3^{3-(n_s-1)}} - \frac{3}{k_2^{3-(n_s-1)} k_3^{3-(n_s-1)}} - \frac{8}{(k_1 k_2 k_3)^{2(4-n_s)/3}} + \left\{ \frac{3}{k_1^{(4-n_s)/3} k_2^{2(4-n_s)/3} k_3^{(4-n_s)}} + (5 \text{ perm}) \right\} \right], \quad (5)$$

and its angular bispectrum is (see for example Yadav & Wandelt 2010; Komatsu 2010)

$$b_{\ell_1 \ell_2 \ell_3}^{ort} = 18 \int_0^\infty dx x^2 \left[-\alpha_{\ell_1}(x) \beta_{\ell_2}(x) \beta_{\ell_3}(x) + (2 \text{ perm}) + \beta_{\ell_1}(x) \gamma_{\ell_2}(x) \delta_{\ell_3}(x) + (5 \text{ perm}) - \frac{8}{3} \delta_{\ell_1}(x) \delta_{\ell_2}(x) \delta_{\ell_3}(x) \right]. \quad (6)$$

Many studies have been performed to constrain f_{nl} , especially for the local and the equilateral cases. The first constraints on f_{nl} were imposed using data sets with low resolution or small sky coverage which led to large uncertainties in f_{nl} . We can report analyses using the *Cosmic Background Explorer* (COBE) data (Komatsu et al. 2002; Santos et al. 2003), MAXIMA data (Cayón et al. 2003; Santos et al. 2003), the *Very Small Array* (VSA) data (Smith et al. 2004), the Archeops data (Curto et al. 2007, 2008) and the BOOMERang data (De Troia et al. 2007; Natoli et al. 2010).

Once the WMAP data were available, significant improvements were achieved in the precision of the estimation of f_{nl}^3 . Many studies have been developed to constrain the f_{nl} using WMAP data and based on different estimators. We can mention the different bispectrum-based estimators (see for example Komatsu et al. 2003; Babich et al. 2004; Fergusson & Shellard 2007; Spergel et al. 2007; Creminelli et al. 2006, 2007; Yadav & Wandelt 2008; Fergusson & Shellard 2009; Komatsu et al. 2009; Smith et al. 2009; Elsner & Wandelt 2009; Bucher et al. 2010; Liguori et al. 2010; Senatore et al. 2010; Smidt et al.

³ The improvement comes from a combination of large sky coverage, high angular resolution and good sensitivity. This combination improves the signal-to-noise ratio of f_{nl} which for the local case is proportional to $\log(\ell_{max})$ (Yadav & Wandelt 2010).

2010; Fergusson et al. 2010a,b; Komatsu et al. 2011; Fergusson & Shellard 2011). The bispectrum is the most natural way to constrain f_{nl} given its linear dependence and the fact that in certain ideal conditions bispectrum-based estimators may be the optimal way to measure f_{nl} . However, given that the data are contaminated by different non-Gaussian parasite signals and in most cases only a fraction of the sky can be used, it is convenient to use additional tools that can help to understand these effects better. We can mention the tests performed using the spherical Mexican hat wavelet (SMHW) (Mukherjee & Wang 2004; Curto et al. 2009a,b, 2011), a HEALPix-based wavelet (Casaponsa et al. 2011a,b), a joint analysis with the SMHW and neural networks (Casaponsa et al. 2011b), needlets (Marinucci et al. 2008; Pietrobon et al. 2009; Rudjord et al. 2009; Pietrobon et al. 2010; Rudjord et al. 2010; Pietrobon et al. 2010; Pietrobon 2010; Cabella et al. 2010), the Minkowski functionals (Hikage et al. 2006; Gott et al. 2007; Hikage et al. 2008; Matsubara 2010; Takeuchi et al. 2010), the N-PDF distribution (Vielva & Sanz 2009, 2010) or a Bayesian approach (Elsner et al. 2010a; Elsner & Wandelt 2010b). Other works use the 3D distribution of matter on large scales (see for example Dalal et al. 2008; Matarrese & Verde 2008; Slosar et al. 2008; Seljak 2009; Desjacques & Seljak 2010; Xia et al. 2010; Baldauf et al. 2011; Hamaus et al. 2011) to constrain the local f_{nl} .

In this paper we focus on the measurement of non-Gaussianity for the previous mentioned shapes using the estimator based on wavelets that has been formerly used to constrain local f_{nl} (Curto et al. 2009a,b, 2010, 2011). We use the technique described by Fergusson et al. (2010a) to produce non-Gaussian maps with the local, equilateral and orthogonal bispectra for WMAP resolution in realistic conditions of partial sky coverage and anisotropic noise. These maps are later used to evaluate the expected values of the wavelet third order moments α_{ijk} for each type of non-Gaussianity. We finally impose constraints on f_{nl} for each shape using the wavelet estimator for the WMAP foreground reduced and raw data maps. As shown later, unresolved point sources produce a significant bias in f_{nl} that should be considered in the analyses of WMAP data and in the forthcoming analyses of Planck data, especially for the equilateral and orthogonal shapes.

This paper is organized as follows. Section 2 presents the non-Gaussian maps that we have used to estimate the quantities needed for this analysis. In Section 3 we present the method and the estimator used in this analysis to constrain f_{nl} . The results of the analysis using WMAP data are presented in Section 4 and the conclusions are presented in Section 5.

2 NON-GAUSSIAN SIMULATIONS

Non-Gaussian Monte Carlo simulations are needed in order to calibrate the wavelet estimator. We have simulated our non-Gaussian maps following the algorithm described by Fergusson et al. (2010a). The non-Gaussian $a_{\ell m}^{NG}$ coefficients can be written in terms of the bispectrum and the

Gaussian $a_{\ell m}^G$ coefficients:

$$a_{\ell m}^{NG} = \frac{1}{6} \sum_{\ell_2, m_2, \ell_3, m_3} b_{\ell\ell_2\ell_3} G_{\ell\ell_2\ell_3}^{m m_2 m_3} \times \begin{pmatrix} \ell & \ell_2 & \ell_3 \\ m & m_2 & m_3 \end{pmatrix} \frac{a_{\ell_2 m_2}^{G*}}{C_{\ell_2}} \frac{a_{\ell_3 m_3}^{G*}}{C_{\ell_3}}. \quad (7)$$

Using the fact that the shape functions of the local, equilateral and orthogonal bispectra are separable, we are able to reduce the number of sums in Eq. 7. This can be done in a straightforward way using Eqs. 2, 4 and 6 in Eq. 7. However, as stated by Hanson et al. (2009); Fergusson et al. (2010a), there are terms that may produce spurious divergences at low multipoles, large enough to affect the power spectrum of the final map. Fergusson et al. (2010a) located the divergent terms and provided equations for the local and equilateral shapes without these terms. A similar procedure can be performed with the orthogonal shape. In the next equations we present the non-Gaussian $a_{\ell m}^{NG}$ coefficients for each of the shapes without divergent terms.

- Local bispectrum

$$a_{\ell m}^{NG} = \int_0^\infty dx x^2 \alpha_\ell(x) \int d^2 \vec{n} Y_{\ell m}^*(\vec{n}) M_\beta(x, \vec{n}) M_\beta(x, \vec{n}) \quad (8)$$

- Equilateral bispectrum

$$a_{\ell m}^{NG} = \int_0^\infty dx x^2 \left\{ -3\alpha_\ell(x) \int d^2 \vec{n} Y_{\ell m}^*(\vec{n}) M_\beta(x, \vec{n}) M_\beta(x, \vec{n}) - 2\delta_\ell(x) \int d^2 \vec{n} Y_{\ell m}^*(\vec{n}) M_\delta(x, \vec{n}) M_\delta(x, \vec{n}) + 6\gamma_\ell(x) \int d^2 \vec{n} Y_{\ell m}^*(\vec{n}) M_\beta(x, \vec{n}) M_\delta(x, \vec{n}) \right\} \quad (9)$$

- Orthogonal bispectrum

$$a_{\ell m}^{NG} = \int_0^\infty dx x^2 \left\{ -9\alpha_\ell(x) \int d^2 \vec{n} Y_{\ell m}^*(\vec{n}) M_\beta(x, \vec{n}) M_\beta(x, \vec{n}) - 8\delta_\ell(x) \int d^2 \vec{n} Y_{\ell m}^*(\vec{n}) M_\delta(x, \vec{n}) M_\delta(x, \vec{n}) + 18\gamma_\ell(x) \int d^2 \vec{n} Y_{\ell m}^*(\vec{n}) M_\beta(x, \vec{n}) M_\delta(x, \vec{n}) \right\} \quad (10)$$

where

$$\alpha_\ell(x) = \frac{2}{\pi} \int_0^\infty k^2 dk g_{T\ell}(k) j_\ell(kx) \quad (11)$$

$$\beta_\ell(x) = \frac{2}{\pi} \int_0^\infty k^2 dk P_\Phi(k) g_{T\ell}(k) j_\ell(kx) \quad (12)$$

$$\gamma_\ell(x) = \frac{2}{\pi} \int_0^\infty k^2 dk P_\Phi^{1/3}(k) g_{T\ell}(k) j_\ell(kx) \quad (13)$$

$$\delta_\ell(x) = \frac{2}{\pi} \int_0^\infty k^2 dk P_\Phi^{2/3}(k) g_{T\ell}(k) j_\ell(kx), \quad (14)$$

$g_{T\ell}(k)$ is the radiation transfer function that can be evaluated using for example the CAMB⁴ or gTFast⁵ software, $P_\Phi(k)$ is the linear power spectrum, $j_\ell(kx)$ is the spherical

⁴ <http://camb.info/>

⁵ <http://gyudon.as.utexas.edu/~komatsu/CRL/index.html>

Table 1. Quadrature in x integration used to compute $a_{\ell m}^{(NG)}$. We have used greater density of points near reionization and recombination as suggested by Smith & Zaldarriaga (2006). Units for x are Mpc.

$0 \leq x \leq 9,500$	64 points, Gauss-Legendre quadrature
$9,500 \leq x \leq 11,000$	128 points, Gauss-Legendre quadrature
$11,000 \leq x \leq 13,800$	64 points, Gauss-Legendre quadrature
$13,800 \leq x \leq 14,600$	170 points, Gauss-Legendre quadrature
$14,600 \leq x \leq 16,000$	42 points, Gauss-Legendre quadrature
$16,000 \leq x \leq 50,000$	42 points, Gauss-Legendre quadrature

Bessel function (of the first kind) and the $M(x, \hat{n})$ maps are defined as

$$M_\alpha(x, \hat{n}) = \sum_{\ell, m} \alpha_\ell(x) a_{\ell, m}^G \frac{Y_{\ell, m}(\hat{n})}{C_\ell} \quad (15)$$

$$M_\beta(x, \hat{n}) = \sum_{\ell, m} \beta_\ell(x) a_{\ell, m}^G \frac{Y_{\ell, m}(\hat{n})}{C_\ell} \quad (16)$$

$$M_\gamma(x, \hat{n}) = \sum_{\ell, m} \gamma_\ell(x) a_{\ell, m}^G \frac{Y_{\ell, m}(\hat{n})}{C_\ell} \quad (17)$$

$$M_\delta(x, \hat{n}) = \sum_{\ell, m} \delta_\ell(x) a_{\ell, m}^G \frac{Y_{\ell, m}(\hat{n})}{C_\ell}. \quad (18)$$

In Figure 1 we plot the power spectrum of the non-Gaussian terms $a_{\ell m}^{(aBB)} \equiv \int_0^\infty dx x^2 \alpha_\ell(x) \int d^2 \vec{n} Y_{\ell m}^*(\vec{n}) M_\beta(x, \vec{n}) M_\beta(x, \vec{n})$, $a_{\ell m}^{(dDD)} \equiv \int_0^\infty dx x^2 \delta_\ell(x) \int d^2 \vec{n} Y_{\ell m}^*(\vec{n}) M_\delta(x, \vec{n}) M_\delta(x, \vec{n})$ and $a_{\ell m}^{(gBD)} \equiv \int_0^\infty dx x^2 \gamma_\ell(x) \int d^2 \vec{n} Y_{\ell m}^*(\vec{n}) M_\beta(x, \vec{n}) M_\delta(x, \vec{n})$. The power spectrum of the Gaussian part is also plotted. We can see that these three terms add negligible extra-power to the full Gaussian plus non-Gaussian map. Once the $a_{\ell m}^{NG}$ terms are computed as a function of the bispectrum and the $a_{\ell m}^G$, the $a_{\ell m}$ coefficients of a simulation with a given f_{nl} can be written as $a_{\ell m} = a_{\ell m}^G + f_{nl} a_{\ell m}^{NG}$.

In this paper we have generated a set of 300 non-Gaussian maps for the local, equilateral and orthogonal f_{nl} . We have assumed a Λ CDM model using the parameters that best fit the WMAP 7-year data (Komatsu et al. 2011). We have computed a power spectrum C_ℓ and a transfer function $g_{T\ell}(k)$ using these parameters as inputs for the CAMB software (Lewis et al. 2000) up to $\ell_{max} = 1535$. The integrals in Eqs. 8, 9 and 10 have been performed using a Gauss-Legendre quadrature. We have used a large density of points near reionization and recombination (see Table 1 for more details). A large number of points has been chosen in order to achieve convergence in the values of the Fisher matrix of the bispectrum. $\sigma_F^2(f_{nl})$ for the three shapes. In Figure 2 the Fisher matrix $\sigma_F^2(f_{nl})$ (Komatsu & Spergel 2001) obtained with the three bispectra is plotted for different ℓ_{max} values. Note that these values are comparable with the values presented for example by Yadav & Wandelt (2010). Once the $a_{\ell m}$ of the simulations with non-Gaussianity are generated, we transform them into WMAP maps for each radiometer by convolving with the appropriate window functions in

the spherical harmonic space and by adding a Gaussian instrumental noise simulation in the real space (Bennett et al. 2003).

3 METHOD

We use an estimator that is based on third-order statistics generated by the different possible combinations of the wavelet coefficient maps of the SMHW evaluated at certain angular scales. See for example Antoine & Vanderghaynst (1998); Martínez-González et al. (2002); Vielva (2007); Martínez-González (2008) for detailed information about this wavelet. This estimator is described and used to search for blind non-Gaussian deviations and constrain local f_{nl} in Curto et al. (2009a,b, 2011).

We consider the same set of angular scales R_i selected in Curto et al. (2011). After evaluating the wavelet coefficient map $w(R_i; \mathbf{b})$ for each angular scale R_i we compute the third order moments q_{ijk} for each possible combination of three angular scales $\{i, j, k\}$. As mentioned in Curto et al. (2011), the expected values of the cubic statistics are linearly proportional to f_{nl}

$$\langle q_{ijk} \rangle_{f_{nl}} = \alpha_{ijk} f_{nl}, \quad (19)$$

where the α_{ijk} term is linearly related to the bispectrum. We evaluate these α_{ijk} quantities for the local, equilateral and orthogonal bispectra by averaging the values of the estimators obtained with the non-Gaussian simulations described in the previous Section. We then compute a χ^2 statistic in order to constrain each f_{nl}

$$\chi^2(f_{nl}) = \sum_{ijk, rst} (q_{ijk}^{obs} - \alpha_{ijk} f_{nl}) C_{ijk, rst}^{-1} (q_{rst}^{obs} - \alpha_{rst} f_{nl}), \quad (20)$$

where q_{ijk}^{obs} is the value of the statistics obtained for the actual data map and C is the covariance matrix among the different statistics q_{ijk} ⁶. The covariance matrix is estimated using the q_{ijk} statistics corresponding to 10,000 WMAP Gaussian simulations. A detailed study described in Curto et al. (2011) was carried out in order to compute correctly its inverse avoiding possible degeneracies. The α_{ijk} statistics are estimated using the set of 300 non-Gaussian simulations transformed into WMAP $V + W$ maps. Although we found analytical expressions for the covariance matrix $C_{ijk, rst}$ and the α_{ijk} quantities (see Curto et al. 2011), those expressions are only valid for the particular ideal case of full sky maps and white isotropic noise. For a realistic case, the analytical expressions become more complicated and the best practical approach to compute those quantities is using simulations.

Finally, this estimator is also applied to a set of Gaussian maps in order to obtain an empirical estimate of the uncertainties of f_{nl} . Additionally we also compute the value of the f_{nl} Fisher matrix using the wavelet coefficients

$$\sigma_F^2(f_{nl}) = \frac{1}{\sum_{ijk, rst} \alpha_{ijk} C_{ijk, rst}^{-1} \alpha_{rst}}. \quad (21)$$

⁶ Note that for this estimator there is no need to subtract any linear term due to the anisotropic noise as in the case of the KSW estimator. The reason is that the non-ideal aspects of the analysis (as the mask, the anisotropic noise, etc.) are included in the covariance matrix and the α_{ijk} coefficients.

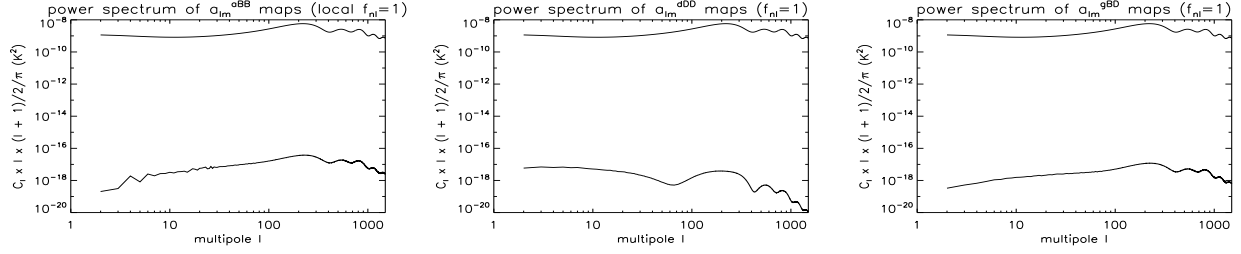


Figure 1. From left to right, the power spectrum of the non-Gaussian $a_{\ell m}^{(aBB)}$, $a_{\ell m}^{(dDD)}$ and $a_{\ell m}^{(gBD)}$ coefficients (lower line) compared with the Gaussian part of the power spectrum (upper line).

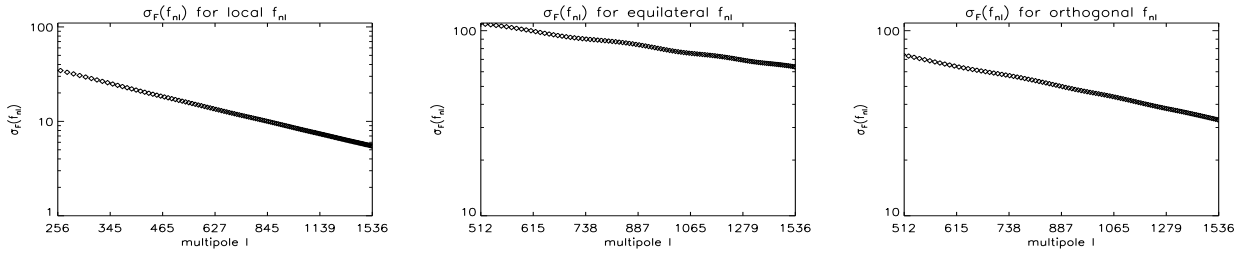


Figure 2. From left to right, the Fisher matrix $\sigma_F(f_{nl})$ versus ℓ_{max} for the local, equilateral and orthogonal bispectra $b_{\ell_1 \ell_2 \ell_3}$ defined in Eqs. 2, 4 and 6.

Table 2. Constraints on the local, equilateral and orthogonal f_{nl} for the clean and raw maps and their uncertainties obtained with the Fisher matrix $\sigma_F(f_{nl})$ and with simulations (RMS).

CASE	raw f_{nl}	clean f_{nl}	$\sigma_F(f_{nl})$	MEAN	RMS
local	25.0	32.5	22.5	0.0	23.00
equilateral	28.0	-53.0	145.0	1.0	156.0
orthogonal	-119.0	-155.0	106.0	0.0	112.00

4 APPLICATION TO WMAP DATA

4.1 Constraints on f_{nl} using WMAP data

We use the combined WMAP 7-year V and W band maps at the HEALPix (Górski et al. 2005) resolution of $N_{side} = 512$. We consider both raw and foreground reduced data maps as Komatsu et al. (2011). The maximum multipole chosen in this analysis is $3N_{side}$ although the noise contamination starts to be significant at $\ell \sim 1000$. For the three shapes we find the best limits on f_{nl} and provide the value of the Fisher and the simulated $\sigma(f_{nl})$. During all the analysis we use the WMAP KQ75 mask (Gold et al. 2011). In Table 2 we summarize our results. We find that for the three cases, the parameters are compatible with zero at 95% CL. We would like to note the different effect that the foregrounds produce on different shapes: whereas it is negative for the local shape, it is positive for the equilateral and orthogonal shapes. For all the cases, $\sigma_F(f_{nl})$ is lower than the value obtained with simulations ($\sim 95\%$ depending on the shape). We think that this small discrepancy is due to the limited number of simulations. We have checked that our estimator is unbiased. We have estimated the f_{nl} values of 100 non-Gaussian simulations with an input $f_{nl} = 100$ and used the remaining 200 non-Gaussian simulations to estimate the

α_{ijk} . The results are $f_{nl}^{loc} = 99.5 \pm 29.5$, $f_{nl}^{eq} = 98 \pm 150$ and $f_{nl}^{ort} = 97 \pm 118$, which are clearly compatible with the input f_{nl} taking into account the expected errors in the mean for the available number of realizations. Our best estimates for the clean maps are:

- Local⁷: $f_{nl} = 32.5 \pm 22.5$ (68% CL)
- Equilateral: $f_{nl} = -53 \pm 145$ (68% CL)
- Orthogonal: $f_{nl} = -155 \pm 106$ (68% CL)

The values match well the results presented by Komatsu et al. (2011) within one sigma error-bars. The differences can be explained by the different sensitivity of the bispectrum and wavelet estimators to the possible non-cosmological residuals present in the data.

4.2 Point source contribution

We have also estimated the contribution of undetected point sources using the source number counts dN/dS derived from de Zotti et al. (2005). We have used point source simulations based on this dN/dS . We have chosen a maximum flux for the bright sources such that the power spectrum for the Q band is compatible with the value provided by the WMAP team, $A_{ps} = 0.0090 \pm 0.0007 \mu K^2 sr$ in antenna units (Larson et al. 2011). We have estimated the

⁷ Using a set of 300 non-Gaussian simulations generated following the procedure by Liguori et al. (2003, 2007) our best estimate is $f_{nl} = 37 \pm 21$ (68% CL). These maps were generated in a different way: the non-Gaussianity is introduced in the primordial curvature perturbation $\Phi(\mathbf{x}) = \Phi_L(\mathbf{x}) + f_{nl}(\Phi_L^2(\mathbf{x}) - \langle \Phi_L^2(\mathbf{x}) \rangle)$ and then extrapolated to the CMB. This process add extra non-Gaussianity at higher moments whereas the procedure used in this paper and in Fergusson et al. (2010a) just adds non-Gaussianity to the third order moments (bispectrum).

best-fitting f_{nl} value for two sets of 1,000 maps. The first set consists of 1,000 Gaussian CMB + noise maps and the second consists of the same Gaussian CMB + noise maps plus the point source maps. For each map with point sources we estimate its best-fitting f_{nl} parameter and compare with the value obtained for the same map without point sources. The difference Δf_{nl} provides an estimate of the impact on f_{nl} due to the unresolved point sources. The point sources add a contribution of $\Delta f_{nl} = 2.5 \pm 3$, $\Delta f_{nl} = 37 \pm 18$ and $\Delta f_{nl} = 25 \pm 14$ for the local, equilateral and orthogonal forms respectively.

To check further these results, we have used an alternative method to estimate the point source contamination to f_{nl} given by the expression

$$\Delta f_{nl} = \frac{\sum_{ijk,rst} \langle q_{ijk} \rangle_{ps} C_{ijk,rst}^{-1} \alpha_{rst}}{\sum_{ijk,rst} \alpha_{ijk} C_{ijk,rst}^{-1} \alpha_{rst}}, \quad (22)$$

where $\langle q_{ijk} \rangle_{ps}$ is the expected value of the third order moments due to the point sources. The results are $\Delta f_{nl} = 2.5$, $\Delta f_{nl} = 38$ and $\Delta f_{nl} = 24$ which agree with the values previously obtained with simulations. Taking into account the point source contribution, our best estimates of f_{nl} are:

- Local: $f_{nl} = 30.0 \pm 22.5$ (68% CL)
- Equilateral: $f_{nl} = -90 \pm 146$ (68% CL)
- Orthogonal: $f_{nl} = -180 \pm 107$ (68% CL)

Fig. 3 contains the histograms of the best-fitting f_{nl} values for each shape corresponding to 1,000 CMB + noise Gaussian simulations and the values of the data after the point source correction. Note that the point sources add a significant contribution to the equilateral and orthogonal shapes. We agree with Komatsu et al. (2011) that the WMAP seven-year data are consistent with Gaussian primordial fluctuations for the three considered shapes. Planck will be able to address this issue with more detail due to its increased sensitivity and power to clean the signal.

5 CONCLUSIONS

We have imposed constraints on primordial non-Gaussianity with the WMAP 7-year data using the wavelet based estimator. In this analysis we have considered the combined V+W maps and the KQ75 mask. In particular, we have focused in three shapes with particular interest for the physics of inflation in the early universe: the local, equilateral and orthogonal bispectra.

We have simulated the non-Gaussian maps for each of the considered shapes and estimated with these simulations the required quantities for our estimator. Our results are compatible with the values obtained by the WMAP team and our uncertainties are very similar to the error bars obtained with the optimal bispectrum estimator (Komatsu et al. 2011).

In addition we have estimated the contribution of the point sources. In the particular case of the local f_{nl} , the contribution is $\Delta f_{nl}^{loc} = 2.5 \pm 3.0$. This is similar to the values obtained by the WMAP team (Komatsu et al. 2011) and its contribution to the parameter is not significant. However we have detected a non-negligible contribution to the equilateral and orthogonal shapes due to the unresolved point sources. In particular, we have found $\Delta f_{nl}^{eq} = 37 \pm 18$

and $\Delta f_{nl}^{ort} = 25 \pm 14$ (68%CL). These large values were already predicted by Komatsu et al. (2011) although they did not provide actual figures. This contribution should be taken carefully into account in future constraints on f_{nl} with WMAP and Planck data. Considering the point sources, our best estimates of f_{nl} are $f_{nl}^{loc} = 30.0 \pm 22.5$, $f_{nl}^{eq} = -90 \pm 146$ and $f_{nl}^{ort} = -180 \pm 107$. The three shapes are compatible with zero at 95% CL. Our conclusion is that the f_{nl} parameters are compatible with zero within the 2σ CL and our results are in agreement with Komatsu et al. (2011).

The wavelet estimator has been tested and carefully checked with the available WMAP data in this and several previous works (Curto et al. 2009a,b, 2011). It is now ready and being upgraded to analyse the forthcoming Planck data. In future works we will also use the wavelet estimator jointly with neural networks to constrain these shapes along the lines of Casaponsa et al. (2011b) where this procedure has been already applied for the local f_{nl} using WMAP data. This later process helps to speed up the calculations since it is not necessary to estimate the covariance matrix of the cubic statistics and it avoids all the possible complications in the computation of the inverse covariance matrix.

ACKNOWLEDGMENTS

The authors are thankful to Eiichiro Komatsu and Michele Liguori for their useful comments that have helped in the production of this paper. The authors thank J. González-Nuevo for providing the dN/dS counts and for his useful comments on unresolved point sources. The authors also thank Biuse Casaponsa, Airam Marcos-Caballero, Sabino Matarrese and Patricio Vielva for useful comments on different computational and theoretical issues on the primordial non-Gaussianity. The authors acknowledge partial financial support from the Spanish Ministerio de Ciencia e Innovación project AYA2010-21766-C03-01, the CSIC-Royal Society joint project with reference 2008GB0012 and the Consolider Ingenio-2010 Programme project CSD2010-00064. A. C. thanks the Universidad de Cantabria for a post-doctoral fellowship. The authors acknowledge the computer resources, technical expertise and assistance provided by the Spanish Supercomputing Network (RES) node at Universidad de Cantabria. We acknowledge the use of Legacy Archive for Microwave Background Data Analysis (LAMBDA). Support for it is provided by the NASA Office of Space Science. The HEALPix package was used throughout the data analysis (Górski et al. 2005).

REFERENCES

- Albrecht A., Steinhardt P. J., 1982, *Physical Review Letters*, 48, 1220
- Antoine J.-P., Vandergheynst P., 1998, *Journal of Mathematical Physics*, 39, 3987
- Arkani-Hamed N., Creminelli P., Mukohyama S., Zaldarriaga M., 2004, *Journal of Cosmology and Astro-Particle Physics*, 4, 1
- Babich D., Creminelli P., Zaldarriaga M., , 2004, *The shape of non-Gaussianities*

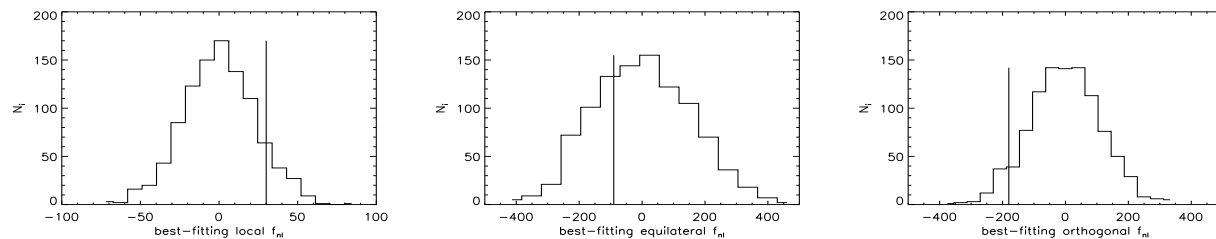


Figure 3. From left to right, the histograms with the best-fitting f_{nl} values obtained for 1,000 Gaussian simulations for the local, equilateral and orthogonal shapes. Vertical lines correspond to the values obtained with the data after taking into account the point source contamination.

- Baldauf T., Seljak U., Senatore L., 2011, *Journal of Cosmology and Astroparticle Physics*, 4, 6
- Bartolo N., Komatsu E., Matarrese S., Riotto A., 2004, *Phys. Rep.*, 402, 103
- Bennett C. L., Hill R. S., Hinshaw G., Nolte M. R., Odegard N., Page L., Spergel D. N., Weiland J. L., Wright E. L., Halpern M., Jarosik N., Kogut A., Limon M., Meyer S. S., Tucker G. S., Wollack E., 2003, *ApJS*, 148, 97
- Bucher M., van Tent B., Carvalho C. S., 2010, *MNRAS*, 407, 2193
- Cabella P., Pietrobon D., Veneziani M., Balbi A., Crittenden R., de Gasperis G., Quercellini C., Vittorio N., 2010, *MNRAS*, 405, 961
- Casaponsa B., Barreiro R. B., Curto A., Martínez-González E., Vielva P., 2011a, *MNRAS*, 411, 2019
- Casaponsa B., Bridges M., Curto A., Barreiro R. B., Hobson, M. P. and Martínez-González E., 2011b, *MNRAS*, accepted for publication, (arXiv:1105.6116)
- Cayón L., Argüeso F., Martínez-González E., Sanz J. L., 2003, *MNRAS*, 344, 917
- Cayón L., Martínez-González E., Argüeso F., Banday A. J., Górski K. M., 2003, *MNRAS*, 339, 1189
- Chen X., Huang M.-x., Kachru S., Shiu G., 2007, *Journal of Cosmology and Astroparticle Physics*, 1, 2
- Cheung C., Fitzpatrick A. L., Kaplan J., Senatore L., Creminelli P., 2008, *Journal of High Energy Physics*, 3, 14
- Creminelli P., Nicolis A., Senatore L., Tegmark M., Zaldarriaga M., 2006, *Journal of Cosmology and Astro-Particle Physics*, 5, 4
- Creminelli P., Senatore L., Zaldarriaga M., 2007, *Journal of Cosmology and Astro-Particle Physics*, 3, 19
- Curto A., Aumont J., Macías-Pérez J. F., Martínez-González E., Barreiro R. B., Santos D., Désert F. X., Tristram M., 2007, *A&A*, 474, 23
- Curto A., Macías-Pérez J. F., Martínez-González E., Barreiro R. B., Santos D., Hansen F. K., Liguori M., Matarrese S., 2008, *A&A*, 486, 383
- Curto A., Martínez-González E., Barreiro R. B., 2009b, *ApJ*, 706, 399
- Curto A., Martínez-González E., Barreiro R. B., 2010, in J. M. Diego, L. J. Goicoechea, J. I. González-Serrano, & J. Gorgas ed., *Highlights of Spanish Astrophysics V, Constraints on the Non-linear Coupling Parameter f_{nl} Using the CMB*. pp 277–+
- Curto A., Martínez-González E., Barreiro R. B., 2011, *MNRAS*, 412, 1038
- Curto A., Martínez-González E., Mukherjee P., Barreiro R. B., Hansen F. K., Liguori M., Matarrese S., 2009a, *MNRAS*, 393, 615
- Dalal N., Doré O., Huterer D., Shirokov A., 2008, *Phys. Rev. D.*, 77, 123514
- De Troia G., Ade P. A. R., Bock J. J., Bond J. R., Borrill J., Boscaleri A., Cabella P., Contaldi C. R., et al. 2007, *ApJL*, 670, L73
- de Zotti G., Ricci R., Mesa D., Silva L., Mazzotta P., Tofolatti L., González-Nuevo J., 2005, *A&A*, 431, 893
- Desjacques V., Seljak U., 2010, *Phys. Rev. D.*, 81, 023006
- Dvali G., Gruzinov A., Zaldarriaga M., 2004, *Phys. Rev. D.*, 69, 023505
- Elsner F., Wandelt B. D., 2009, *ApJS*, 184, 264
- Elsner F., Wandelt B. D., 2010b, *ApJ*, 724, 1262
- Elsner F., Wandelt B. D., Schneider M. D., 2010a, *A&A*, 513, A59+
- Fergusson J., Shellard E. S., 2011, preprint (arXiv:1105.2791)
- Fergusson J. R., Liguori M., Shellard E. P. S., 2010a, *Phys. Rev. D*, 82, 023502
- Fergusson J. R., Liguori M., Shellard E. P. S., 2010b, preprint (arXiv:1006.1642)
- Fergusson J. R., Regan D. M., Shellard E. P. S., 2010c, preprint (arXiv:1008.1730)
- Fergusson J. R., Shellard E. P. S., 2007, *Phys. Rev. D*, 76, 083523
- Fergusson J. R., Shellard E. P. S., 2009, *Phys. Rev. D*, 80, 043510
- Gold B., Odegard N., Weiland J. L., Hill R. S., Kogut A., et al. 2011, *ApJS*, 192, 15
- Górski K. M., Hivon E., Banday A. J., Wandelt B. D., Hansen F. K., Reinecke M., Bartelmann M., 2005, *ApJ*, 622, 759
- Gott J. R., Colley W. N., Park C.-G., Park C., Mugnolo C., 2007, *MNRAS*, 377, 1668
- Guth A. H., 1981, *Phys. Rev. D*, 23, 347
- Hamaus N., Seljak U., Desjacques V., 2011, preprint (arXiv:1104.2321)
- Hanson D., Smith K. M., Challinor A., Liguori M., 2009, *Phys. Rev. D.*, 80, 083004
- Hikage C., Komatsu E., Matsubara T., 2006, *ApJ*, 653, 11
- Hikage C., Matsubara T., Coles P., Liguori M., Hansen F. K., Matarrese S., 2008, *MNRAS*, 389, 1439
- Komatsu E., 2009, in American Astronomical Society Meeting Abstracts #213 Vol. 41 of *Bulletin of the American Astronomical Society, Prospects for Gaussianity Tests of Inflation with SPT and ACT*
- Komatsu E., 2010, *Classical and Quantum Gravity*, 27,

- 124010
 Komatsu E., Dunkley J., Nolta M. R., Bennett C. L., Gold B., Hinshaw G., Jarosik N., Larson D., Limon M., Page L., Spergel D. N., Halpern M., Hill R. S., Kogut A., Meyer S. S., Tucker G. S., Weiland J. L., Wollack E., Wright E. L., 2009, *ApJS*, 180, 330
 Komatsu E., Kogut A., Nolta M. R., Bennett C. L., Halpern M., Hinshaw G., Jarosik N., Limon M., Meyer S. S., Page L., Spergel D. N., Tucker G. S., Verde L., Wollack E., Wright E. L., 2003, *ApJS*, 148, 119
 Komatsu E., Smith K. M., Dunkley J., Bennett C. L., Gold B., et al. 2011, *ApJS*, 192, 18
 Komatsu E., Spergel D. N., 2001, *Phys. Rev. D*, 63, 063002
 Komatsu E., Spergel D. N., Wandelt B. D., 2005, *ApJ*, 634, 14
 Komatsu E., Wandelt B. D., Spergel D. N., Banday A. J., Górski K. M., 2002, *ApJ*, 566, 19
 Langlois D., Renaux-Petel S., Steer D. A., Tanaka T., 2008, *Phys. Rev. D*, 78, 063523
 Larson D., Dunkley J., Hinshaw G., Komatsu E., Nolta M. R., et al. 2011, *ApJS*, 192, 16
 Lewis A., Challinor A., Lasenby A., 2000, *ApJ*, 538, 473
 Liguori M., Matarrese S., Moscardini L., 2003, *ApJ*, 597, 57
 Liguori M., Yadav A., Hansen F. K., Komatsu E., Matarrese S., Wandelt B., 2007, *Phys. Rev. D*, 76, 105016
 Liguori M., Sefusatti E., Fergusson J. R., Shellard E. P. S., 2010, *Advances in Astronomy*, 2010
 Lin C., 2009, preprint (arXiv:0908.4168)
 Linde A. D., 1982, *Physics Letters B*, 108, 389
 Linde A. D., 1983, *Physics Letters B*, 129, 177
 Lyth D. H., Ungarelli C., Wands D., 2003, *Phys. Rev. D*, 67, 023503
 Marinucci D., Pietrobon D., Balbi A., Baldi P., Cabella P., Kerkycharian G., Natoli P., Picard D., Vittorio N., 2008, *MNRAS*, 383, 539
 Martínez-González E., 2008, preprint (arXiv:0805.4157)
 Martínez-González E., Gallegos J. E., Argüeso F., Cayón L., Sanz J. L., 2002, *MNRAS*, 336, 22
 Matarrese S., Verde L., 2008, *ApJL*, 677, L77
 Matsubara T., 2010, *Phys. Rev. D*, 81, 083505
 Mukhanov V. F., Feldman H. A., Brandenberger R. H., 1992, *Phys. Rep.*, 215, 203
 Mukherjee P., Wang Y., 2004, *ApJ*, 613, 51
 Natoli P., De Troia G., Hikage C., Komatsu E., Migliaccio et al., 2010, *MNRAS*, 408, 1658
 Pietrobon D., 2010, *Memorie della Societa Astronomica Italiana Supplementi*, 14, 278
 Pietrobon D., Balbi A., Cabella P., Gorski K. M., 2010, *ApJ*, 723, 1
 Pietrobon D., Cabella P., Balbi A., Crittenden R., de Gasperis G., Vittorio N., 2010, *MNRAS*, 402, L34
 Pietrobon D., Cabella P., Balbi A., de Gasperis G., Vittorio N., 2009, *MNRAS*, 396, 1682
 Rudjord Ø., Hansen F. K., Lan X., Liguori M., Marinucci D., Matarrese S., 2009, *ApJ*, 701, 369
 Rudjord Ø., Hansen F. K., Lan X., Liguori M., Marinucci D., Matarrese S., 2010, *ApJ*, 708, 1321
 Santos M. G., Heavens A., Balbi A., Borrill J., Ferreira P. G., Hanany S., Jaffe A. H., Lee A. T., Rabii B., Richards P. L., Smoot G. F., Stompor R., Winant C. D., Wu J. H. P., 2003, *MNRAS*, 341, 623
 Seljak U., 2009, *Physical Review Letters*, 102, 021302
 Senatore L., Smith K. M., Zaldarriaga M., 2010, *Journal of Cosmology and Astro-Particle Physics*, 1, 28
 Silverstein E., Tong D., 2004, *Phys. Rev. D*, 70, 103505
 Slosar A., Hirata C., Seljak U., Ho S., Padmanabhan N., 2008, *Journal of Cosmology and Astro-Particle Physics*, 8, 31
 Smidt J., Amblard A., Byrnes C. T., Cooray A., Heavens A., Munshi D., 2010, *Phys. Rev. D*, 81, 123007
 Smith K. M., Senatore L., Zaldarriaga M., 2009, *Journal of Cosmology and Astro-Particle Physics*, 9, 6
 Smith K. M., Zaldarriaga M., 2006, *ArXiv Astrophysics e-prints*
 Smith S., Rocha G., Challinor A., Battye R. A., et al. 2004, *MNRAS*, 352, 887
 Spergel D. N., Bean R., Doré O., Nolta M. R., Bennett C. L., Dunkley J., Hinshaw G., Jarosik N., et al. 2007, *ApJS*, 170, 377
 Starobinskiĭ A. A., 1979, *Soviet Journal of Experimental and Theoretical Physics Letters*, 30, 682
 Takeuchi Y., Ichiki K., Matsubara T., 2010, *Phys. Rev. D*, 82, 023517
 Verde L., Wang L., Heavens A. F., Kamionkowski M., 2000, *MNRAS*, 313, 141
 Vielva P., 2007, in *Society of Photo-Optical Instrumentation Engineers (SPIE) Conference Series Vol. 6701 of Society of Photo-Optical Instrumentation Engineers (SPIE) Conference Series, Probing the Gaussianity and the statistical isotropy of the CMB with spherical wavelets*
 Vielva P., Sanz J. L., 2009, *MNRAS*, 397, 837
 Vielva P., Sanz J. L., 2010, *MNRAS*, 404, 895
 Xia J., Viel M., Baccigalupi C., De Zotti G., Matarrese S., Verde L., 2010, *ApJL*, 717, L17
 Yadav A. P. S., Wandelt B. D., 2008, *Physical Review Letters*, 100, 181301
 Yadav A. P. S., Wandelt B. D., 2010, *Advances in Astronomy*, 2010